viruses

MDPI

Article

Coronavirus RNA Synthesis Takes Place within Membrane-Bound Sites

Nicole Doyle, Jennifer Simpson, Philippa C. Hawes and Helena J. Maier *

The Pirbright Institute, Ash Road, Woking GU24 0NF, UK; nicole.doyle@pirbright.ac.uk (N.D.); jennifer.simpson@pirbright.ac.uk (J.S.); pippa.hawes@pirbright.ac.uk (P.C.H.)
* Correspondence: helena.maier@pirbright.ac.uk

Abstract: Infectious bronchitis virus (IBV), a gammacoronavirus, is an economically important virus to the poultry industry, as well as a significant welfare issue for chickens. As for all positive strand RNA viruses, IBV infection causes rearrangements of the host cell intracellular membranes to form replication organelles. Replication organelle formation is a highly conserved and vital step in the viral life cycle. Here, we investigate the localization of viral RNA synthesis and the link with replication organelles in host cells. We have shown that sites of viral RNA synthesis and virus-related dsRNA are associated with one another and, significantly, that they are located within a membrane-bound compartment within the cell. We have also shown that some viral RNA produced early in infection remains within these membranes throughout infection, while a proportion is trafficked to the cytoplasm. Importantly, we demonstrate conservation across all four coronavirus genera, including SARS-CoV-2. Understanding more about the replication of these viruses is imperative in order to effectively find ways to control them.

Keywords: infectious bronchitis virus; IBV; replication; bromouridine; viral RNA synthesis; replication organelle; 229E; SARS-CoV-2; PDCoV

check for updates

Citation: Doyle, N.; Simpson, J.; Hawes, P.C.; Maier, H.J. Coronavirus RNA Synthesis Takes Place within Membrane-Bound Sites. *Viruses* **2021**, *13*, 2540. https://doi.org/10.3390/v13122540

Academic Editor: Feng Li

Received: 4 November 2021
Accepted: 15 December 2021
Published: 17 December 2021

Publisher's Note: MDPI stays neutral with regard to jurisdictional claims in published maps and institutional affiliations.

Copyright: © 2021 by the authors. Licensee MDPI, Basel, Switzerland. This article is an open access article distributed under the terms and conditions of the Creative Commons Attribution (CC BY) license (https://creativecommons.org/licenses/by/4.0/).

1. Introduction

Coronaviruses (CoVs) are an important family of positive strand RNA (+RNA) viruses with a wide host range. In humans, some strains of these viruses, such as the human coronavirus (HCoV) 229E, can cause the common cold; however, there are now three CoVs that are more pathogenic and cause higher fatality rates. Until 2019, severe acute respiratory syndrome coronavirus (SARS-CoV) and Middle East respiratory syndrome coronavirus (MERS-CoV), which were initially isolated in China and Saudi Arabia, respectively [1,2], were the most well-known zoonotic viruses in the coronavirus family. However, the emergence of SARS-CoV-2, causing global mortalities (over 5 million people at the time of writing [3]) and the shut-down of normal life, has brought a focus on the danger of zoonotic viruses, and in particular this virus family [4]. Apart from human viruses, coronaviruses cause disease in a range of animal species. Several of these viruses are of economic importance as they cause infections and loss of income in the global agriculture industry. These include viruses such as porcine epidemic diarrhea virus (PEDV), porcine deltacoronavirus (PDCoV), bovine coronavirus (BCoV), and avian infectious bronchitis virus (IBV). As has recently been highlighted, studying these viruses is of vital importance. Much work on the CoV family over recent years has been focused on understanding how they interact with the host cell, including a key part of their life cycle, the induction of membrane rearrangements, or replication organelles (Ros).

As obligate intracellular parasites, viruses rely on their host cells to provide not only a site for replication, but much of the cellular machinery required to produce new virus particles. All +RNA viruses induce the rearrangement of intracellular membranes to form Ros [5–7]. These viral Ros have been shown to be the site of viral RNA synthesis [8,9]; however, it is probable that they offer other benefits to the virus. The ROs are likely to

provide a way to shield replicative intermediates, which would otherwise be recognized by cellular defenses and spark an innate immune response [10,11]. It has recently been shown that ROs could be a site of local ATP production for the energy-intensive process of RNA synthesis, which takes place there [12]. The structures formed vary between virus families, but they share similarities in structures, such as convoluted membranes, double membrane vesicles (DMVs), and spherules [13,14]. Several viruses, such as toroviruses [15], hepatitis C virus (HCV, [16]) and picornaviruses, such as foot and mouth disease virus (FMDV [17]), induce the formation of tubules or paired membranes as well as single-membrane vesicles, DMVs, or multi-lamellar vesicles. In enterovirus infections, single-membrane tubules transform into DMVs and multilamellar vesicles over the course of infection [18,19], using endoplasmic reticulum (ER) and Golgi membranes to initiate the formation of these structures [20]. A different structure induced by many other +RNA viruses are spherules or invaginated vesicles. These structures are smaller than DMVs and are pinched out from various intracellular membranes, but since they remain bound to that membrane, they possess a channel which connects their interior to the cytoplasm. Viruses that induce spherule formation include flaviviruses [21–23], nodaviruses [24], bromoviruses [25], and alphaviruses such as Semliki Forest virus (SFV). In the case of SFV ROs, the spherules, and the cytopathic vacuoles which contain them have been shown to be the site of viral RNA synthesis [26–28]. For flock house nodavirus (FHV), spherules have been found to form from the mitochondrial membrane [29] and these structures have also been shown to be the site of viral RNA synthesis, containing bundles of dsRNA [30,31].

The possibility of antiviral therapies targeting the ROs has meant an increased attraction for understanding this part of the viral life cycle in recent years. Until very recently, the structures of ROs formed by the CoV family were split into the alpha- and beta-CoVs and the gamma- and delta-CoVs. The alpha- and beta-CoVs were known to induce convoluted membranes and DMVs [9,32–35], and while DMVs are also produced by gamma- and delta-CoVs, these were seen alongside areas of tightly paired ER membranes called zippered ER (zER) and small double membrane spherules, which, in IBV infected cells, have been shown to remain tethered via an open neck to the zER [36,37]. However, it has recently been shown that alpha- and beta-CoVs induce spherules, although with some morphological differences. They are formed to a lesser extent, and while some spherules appear to be connected to the convoluted membrane, many more were seen as sealed structures. While some sealed spherule structures were seen in IBV infection in the later study, this was to a lesser extent [8]. The significance of these differences between structures is not yet clear and is the source of further investigation.

As ROs have long been purported to provide a site for viral RNA synthesis, a key point for investigation has been in understanding exactly where the sites of viral replication are within the cell, and the involvement of ROs in the process. For SARS-CoV, it has been shown using biochemical methods in vitro that sites of viral RNA synthesis are protected by membranes, possibly within DMVs [38], and dsRNA signal was shown to be associated with DMVs and CM using immunostaining [39]. SARS-CoV-2 DMVs have recently been shown to contain RNA filaments consistent with the size of dsRNA [40]. It is assumed that DMVs in mouse coronavirus (MHV) play a role in viral RNA synthesis since mutations in one of the non-structural proteins, nsp4, affects both DMV formation and viral RNA synthesis [41,42]. DMVs were known to be necessary for viral replication [43] and while DMVs have long been associated with sites of viral RNA synthesis [9], this theory was always hampered by the fact that DMVs were shown to be closed compartments with no way for newly synthesized viral RNA to escape for packaging and egress. However, DMVs have now been shown to be a site of viral RNA synthesis [8] and further recent findings demonstrated a small number of transient pores in the membranes of MHV DMVs, allowing egress of newly synthesized viral RNA [44]. The role of spherules remains to be elucidated.

The gammacoronavirus, IBV is a virus of economic importance to the global poultry industry, causing a highly contagious respiratory disease of chickens and other poultry.

Infection results in reduced quantity and quality of eggs and meat and has an impact on animal welfare as well. Recent work has elucidated the role of ROs in viral RNA synthesis and suggested a pathway for nascent RNA to leave the DMV via a molecular pore [44]. However, conclusive proof of viral RNA synthesis occurring within the DMV was still lacking and the possibility remained that synthesis was taking place on the outer surface of DMVs. Here, we show that IBV viral RNA synthesis takes place within membrane-bound compartments, and we demonstrate that this is conserved across all four genera of the CoV family.

2. Materials and Methods

2.1. Cells and Viruses

Avian DF1 cells (LGC Standards Ltd., Teddington, UK) were maintained in DMEM (Sigma Aldrich, Gillingham, UK) supplemented with 10% FBS (Sigma Aldrich, Gillingham, UK) at 37 °C 5% CO_2. IBV (strain BeauR [45]) infections were carried out in 1 × BES medium (MEM), 0.3% tryptose phosphate broth, 0.2% bovine serum albumin, 20 mM *N*,*N*-Bis(2-hydroxyethyl)-2-aminoethanesulfonic acid (BES), 0.21% sodium bicarbonate, 2 mM L-glutamine, 250 U/mL nystatin, 100 U/mL penicillin, and 100 U/mL streptomycin). Huh7 cells (ATCC, Manassas, VA, USA) were maintained in DMEM supplemented with 10% FBS. Human coronavirus 229E (HCoV 299E (UK Health Security Agency, Didcot, UK) infections were carried out in DMEM + 2% FBS. VeroE6 cells (LGC Standards Ltd., Teddington, UK) were maintained in DMEM supplemented with 10% FBS. SARS-CoV-2 (strain hCov-19/England/02/2020, kindly provided by Prof Miles Carroll, UK Health Security Agency) infections were carried out in DMEM + 2% FBS. Porcine LLC-PK1 cells (ATCC CL-101 [46]) were maintained in DMEM supplemented with 10% FBS. PD-CoV (strain OH-FD22, kindly provided by Prof Linda Saif, Ohio State University, [47,48]), infection was carried out in EMEM + 1% HEPES, 1% non-essential amino acids, 1% antibiotic/antimycotic, and 0.25 µg/mL trypsin. In all cases, cells were inoculated with the virus for 1 h, after which time the inoculum was replaced with infection media, specific to each virus. Cells were then incubated until specified timepoints.

2.2. Labeling of Nascent Viral RNA with Bromouridine

Cells seeded onto glass coverslips were infected as in Section 2.1. Cells were then treated with 2 mM (or 4 mM for HcoV 229E) bromouridine (BrU; Sigma Aldrich) and 15 µM actinomycin D (ActD; Sigma Aldrich) at 30 min prior to each timepoint. Cells were washed in PBS, fixed in RNase-free paraformaldehyde (pfm) at each timepoint, then labeled as in Section 2.3.

For pulse chase experiments, cells were pulsed with BrU and ActD for 1 h at concentrations previously used. After this time, control cells were fixed in RNase-free pfm, while the rest were chased with 50 µM uridine (Sigma Aldrich) to out-compete the labeled BrU. Cells were incubated in uridine and ActD until 24 hpi then fixed as above and labeled as in Section 2.3.

2.3. Immunofluorescence Labeling

Cells seeded onto glass coverslips were mock-infected or infected as laid out in Sections 2.1 and 2.2. At each timepoint, cells were washed in PBS then fixed for 15 min in 4% pfm in PBS at room temperature. Cells were permeabilized in 0.1% Triton X-100 in PBS for 15 min, or 0.25% digitonin (BioVision Inc., Milpitas, CA, USA) in PBS for 10 min, then incubated in blocking buffer (0.1% fish gelatin, Sigma Aldrich, in PBS) for 1 h. Primary antibodies specific for proteins of interest (Table 1) were diluted in blocking buffer and incubated on cells for 1 h. After washing, Alexa Fluor secondary antibody (ThermoFisher Scientific, Waltham, MA, USA) in blocking buffer was incubated on cells for 1 h, followed by washing, labeling of nuclei using 4′,6-diamidino-2-phenylindole (DAPI; Sigma Aldrich) or ToPro3 (ThermoFisher Scientific, Waltham, MA, USA), and mounting onto glass slides with Vectashield (Vector Labs, Peterborough, UK).

Table 1. Table showing antibodies used in this paper.

Antibody Name in Text	Antibody Target	Source
dsRNA	J2 dsRNA	Scicons (English and Scientific Consulting, Budapest, Hungary)
Nsp12	IBV RdRp (nsp12)	Maier et al. mBio '13
IBV	IBV structural proteins (S, M, and N)	Abcam
PDI	PDI	Enzo
b-tubulin	b-tubulin	ThermoFisher
BrU	Anti-Bromodeoxyuridine	Roche, Sigma
229E N	HCoV 229E N protein	MRC PPU Reagents and Services
SARS2 N	SARS-CoV2 N protein	MRC PPU Reagents and Services
PDCoV N	PDCoV NP antigen	2B Scientific

For labeling of BrU samples, in order to prevent loss of the BrU signal, immunofluorescence (IF) labeling was promptly carried out in an RNase-free environment in the presence of RNasin at 0.133 U/mL (Promega, Southampton, UK; [49]).

Cells were visualized using a Leica CLSM SP5, SP8 or Stellaris 5 microscope (Leica Microsystems, Milton Keynes, UK). Super-resolution (stimulated emission depletion (STED)) microscopy was performed using a Leica TCS SP8 STED 3X microscope with inverted stand. STED Images were deconvolved using Huygens Professional software 18.10 (Scientific Volume Imaging, Hilversum, The Netherlands). Figures were assembled using Adobe Photoshop CS6.

3. Results

3.1. DsRNA Is Found in Membrane-Bound Compartments

We have shown previously over the course of the IBV life cycle that nsp12, the viral RNA-dependent RNA polymerase (RdRp), does not colocalize with dsRNA [37]. The role of dsRNA is still a source of interest, but it is most likely to be a replicative intermediate, formed during the replication of the viral genome. Interestingly, dsRNA has recently been shown to be largely negative-sense viral RNA [50]. It has been shown in SARS-CoV infections, that dsRNA is found within DMVs, which are quite likely to store it, hidden from detection by intracellular pattern recognition receptors [39]. The formation of dsRNA is a well conserved step across +RNA virus families, so we sought to understand whether dsRNA is protected within membrane-bound compartments in IBV infection using different permeabilization agents. Digitonin is a weak permeabilizing agent, which can be used at low concentrations to selectively permeabilize the plasma membrane, but not intracellular membranes, while Triton X-100 (TX100) permeabilizes all cellular membranes. Mock-infected DF1 cells were permeabilized with TX100 (Figure 1, top) or digitonin (Figure 1, bottom), then labeled with antibodies specific for PDI and tubulin. Tubulin proteins are found in the cytoplasm, as such tubulin labeling was visible upon either TX100 or digitonin permeabilization. In contrast, labeling of PDI, the intra-lumenal ER protein was lost with digitonin treatment, as the antibody was prevented from accessing its target. DF1 cells infected with IBV and fixed at timepoints during the infection cycle as indicated (Figure 1) were similarly processed. On the top row, cells permeabilized with TX100 clearly showed both nsp12 (green) and dsRNA (red) labeling, with the dsRNA labeling increasing markedly over the course of infection. However, when cells were permeabilized with digitonin (Figure 1, bottom row), dsRNA was no longer visible in the cells, indicating that it was held within an intracellular membrane and, therefore, inaccessible to the antibody.

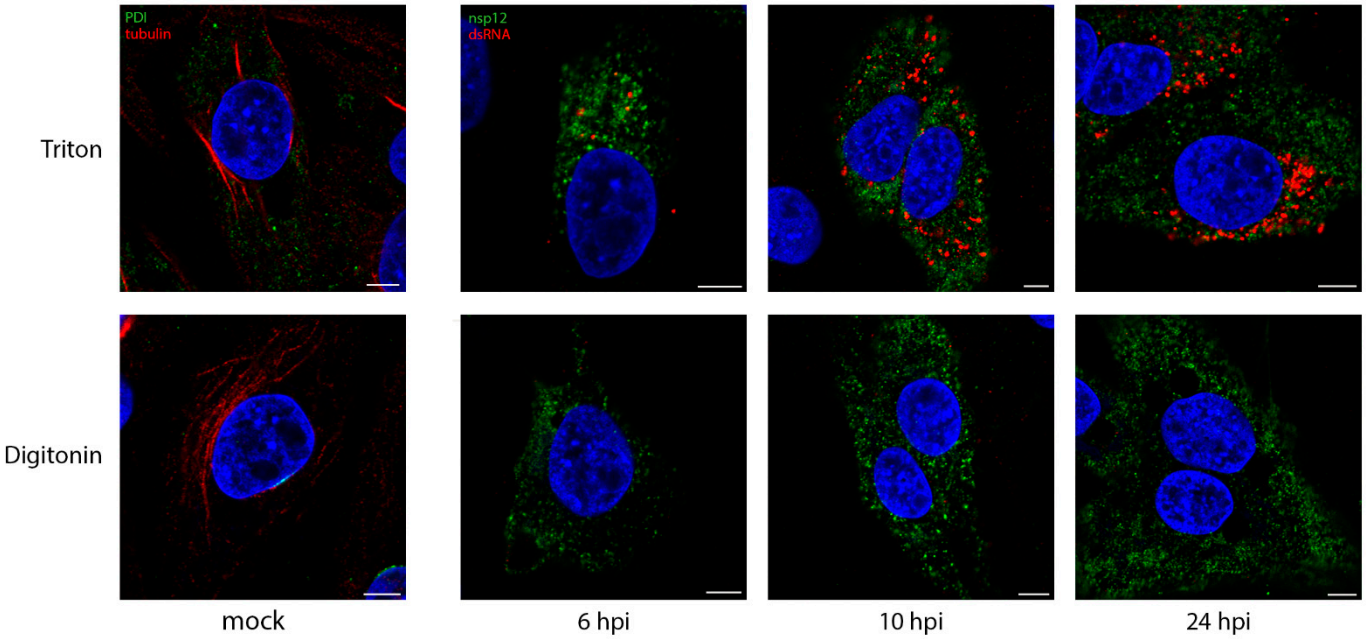

Figure 1. DsRNA is contained within a membrane-bound compartment whilst nsp12 is exposed to the cytoplasm. DF1 cells were infected with IBV and fixed at the indicated times post infection. Cells were permeabilized with either Triton X-100 (all membranes permeabilized; top row), or digitonin (plasma membrane permeabilized only; bottom row). Cells were labeled with dsRNA (red) and nsp12 (green), or for the mock control (first column), tubulin (red) and PDI (green). Nuclei are labeled blue with DAPI (blue). Scale bars represent 5 μm. Images are representative of 3 independent replicates.

In comparison, nsp12 staining was unaffected when cells were permeabilized with digitonin (Figure 1), indicating that it is not contained within a membrane, but is possibly free in the cytoplasm or on the cytoplasmic face of a membrane.

3.2. DsRNA Is Closely Associated with Sites of Viral RNA Synthesis

Knowing that dsRNA was likely within the DMVs, we sought to understand how it associated with sites of viral RNA synthesis. The uridine analog bromouridine (BrU) was incorporated into the nascent viral RNA. DF1 cells were infected with IBV then incubated in media containing BrU for 30 min prior to fixation to provide a snapshot of RNA synthesis at that timepoint. The cellular transcription inhibitor, Actinomycin D (ActD) was used to selectively inhibit cellular transcription to allow visualization of sites of active viral RNA synthesis (Figure S1). Starting at 4 hpi, sites of viral RNA synthesis (Figure 2, green) were detected as small foci localized in the perinuclear region. As infection progressed, these sites of viral RNA synthesis increased in size and distribution around the cell, although often retaining their perinuclear distribution. A similar pattern was observed for both nsp12 and dsRNA labeling (red); however, while nsp12 labeling was generally diffused over the cytoplasm, dsRNA labeling remained punctate and tended to accumulate in perinuclear regions, especially earlier in infection (Figure 2b). Over the course of infection with IBV, nsp12 did not colocalize with BrU (Figure 2a). This was surprising as we would expect the viral RdRp to be at sites of viral RNA synthesis, however no colocalization could be found, even when analyzed in 3D (Figure S2 and Video S1) or using super resolution microscopy (Figure 2c). In contrast, dsRNA, appeared to exhibit a low level of colocalization or overlap with BrU signal at earlier timepoints, particularly in larger foci and as infection progressed, the overlap appeared to increase (Figure 2b). Using super-resolution microscopy, we confirmed that rather than tightly colocalizing, dsRNA and BrU signal were instead in close association with each other (Figure 2c and Video S2). These results showed that dsRNA, while not appearing to be completely colocalized with BrU-labeled nascent RNA, was closely associated with these sites of viral RNA synthesis.

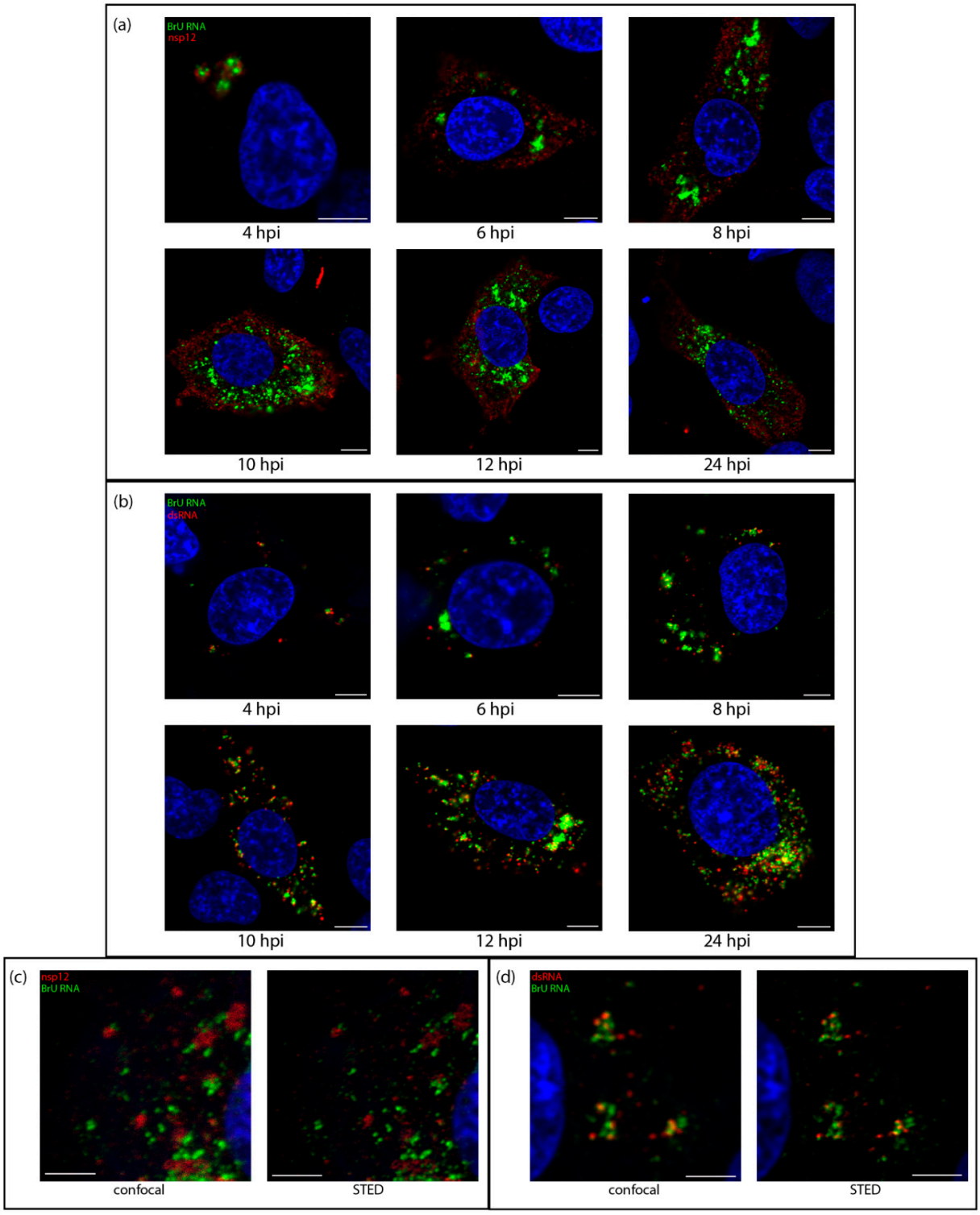

Figure 2. Sites of viral RNA synthesis are associated with dsRNA, but do not colocalize with nsp12. DF1 cells were infected with IBV and 30 min prior to fixation treated with BrU and ActD. Cells were fixed at the indicated time points post infection and labeled with antibodies against BrU (green) and (**a**) nsp12 (red) or (**b**) dsRNA (red). Nuclei are labeled with DAPI (blue). Scale bars represent 5 μm. Images are representative of three independent replicates; (**c**,**d**) cells were treated as in (**a**,**b**), fixed at 10 hpi and labeled for BrU (green) and (**c**) nsp12 or (**d**) dsRNA (red) and ToPro3 (blue) for the nuclei. A confocal image was captured followed by a super-resolution image, which was captured using a STED microscope, then deconvolved. Scale bars represent 3 μm.

3.3. Sites of Viral RNA Synthesis Are Membrane-Protected

Snijder et al. [8] showed that sites of viral RNA synthesis are associated strongly with ROs, in particular they showed they were more strongly associated with DMVs. While they subsequently showed that DMVs have a pore which would allow for the egress of newly synthesized viral RNA, the question of pinpointing nascent viral RNA within these structures remained [44]. Here it has been demonstrated that sites of IBV viral RNA synthesis and dsRNA are closely associated, rather than precisely colocalized. Since we had already shown that dsRNA was within membrane-bound compartments, this left the question open as to whether the sites of viral RNA synthesis might be on the outside of these vesicles. DF1 cells were infected and treated with BrU and ActD as before, followed by IF labeling using either TX100 or digitonin permeabilization. As in previous experiments, the labeling pattern of newly synthesized viral RNA in TX100-permeabilized cells increased through the course of infection from smaller puncta to larger foci, mostly centered in perinuclear regions (Figure 3, top row). Through the course of infection, nsp12 signal was unaffected by digitonin permeabilization (Figures 1 and 3). Strikingly however, much of the BrU signal at these timepoints was not detectable following digitonin permeabilization (Figure 3, bottom row). Although some newly synthesized viral RNA was found in the cytoplasm, this observation indicated that a large proportion of newly synthesized viral RNA was bound within a membrane. Overall viral RNA labeling followed a very similar staining pattern to dsRNA (as seen in Figure 1) and suggested that nascent viral RNA was located within the same membrane-bound compartments as dsRNA.

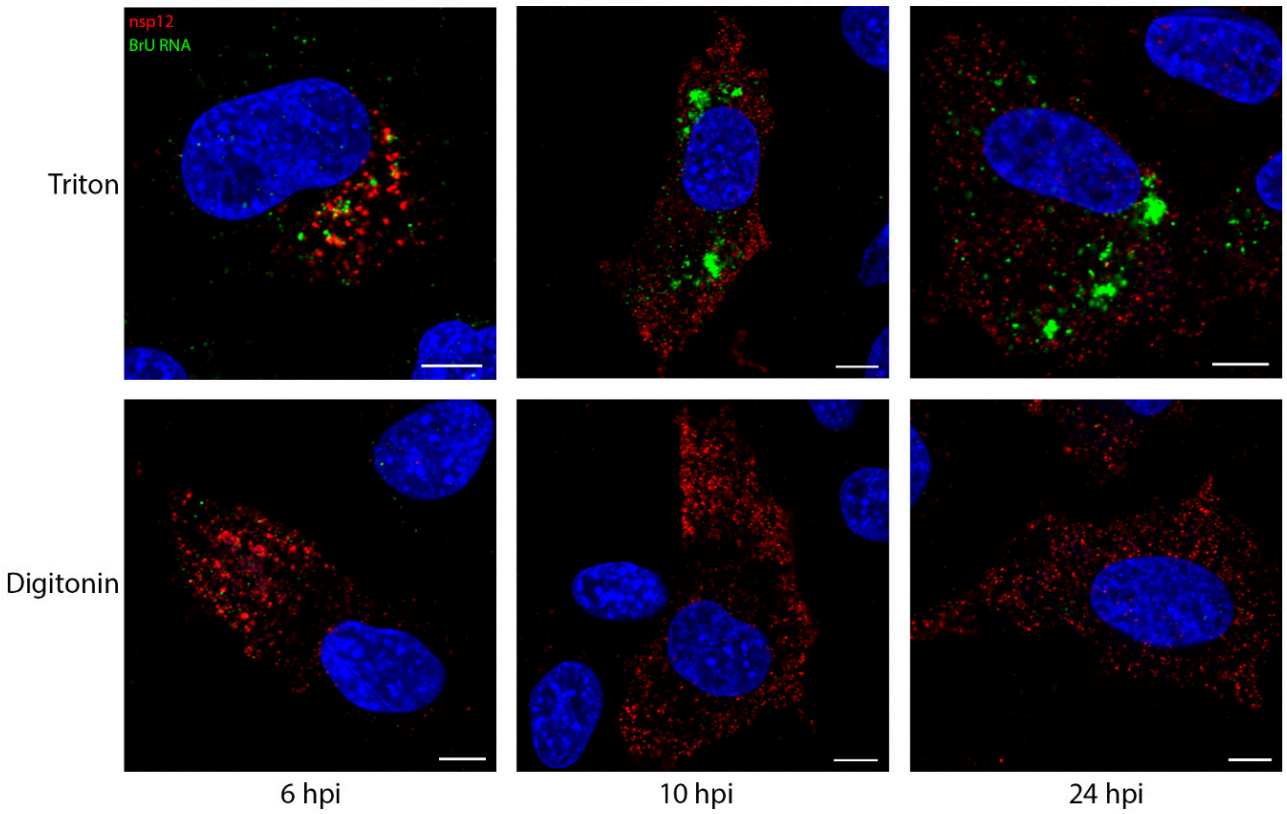

Figure 3. Viral RNA synthesis takes place in a membrane-bound compartment. DF1 cells were infected with IBV. 30 min prior to fixation, cells were treated with BrU and ActD. Cells were fixed at the indicated times post infection. Cells were permeabilized with Triton X-100 (all membranes; top row) or digitonin (plasma membrane; bottom row) then labeled for nsp12 (red) and BrU (green), with nuclei labeled with DAPI (blue). Scale bars represent 5 µm. Images are representative of 3 independent replicates.

3.4. Viral RNA Is Transported to the Cytoplasm Later in Infection

To trace the fate of viral RNA synthesized early in infection and find out whether viral RNA produced within membrane-bound compartments is transported to the cytoplasm, cells were successively exposed to labeled uridine in the form of bromouridine (pulse) and then to unlabeled uridine (chase). In these pulse-chase experiments, viral RNA produced between 7–8 hpi was labeled with BrU as before, followed by a chase with excess unlabeled uridine until fixation at 24 hpi. The localization of viral RNA at 8 hpi was in cytoplasmic puncta, consistent with earlier observations (Figure 4a, left). When this viral RNA was chased to 24 hpi, it was found localized in large cytoplasmic puncta, but also diffuse within the cytoplasm. (Figure 4a, right). To gain further information, cells were permeabilized with TX100 or digitonin as before. In control cells fixed at 8 hpi and permeabilized with TX100 or digitonin, labeling of the viral RNA was as before (Figure 4b, left). In the pulse-chased samples, the large foci of BrU-labeled RNA were no longer visible. However, the diffuse cytoplasmic signal was still detected (Figure 4b, right). Therefore, one pool of RNA was located within a membrane-bound compartment and a second was free in the cytoplasm. To investigate whether the cytoplasmic viral RNA might be in the process of being packaged, we looked to confirm that it colocalizes with viral structural proteins. Therefore, cells were labeled with an antibody specific for viral structural proteins (spike, membrane, and nucleocapsid proteins). The colocalization between these markers (Figure 4c, top) indicates that the diffuse cytoplasmic staining pattern of BrU-labeled viral RNA is associated with structural proteins. In contrast, dsRNA was shown to colocalize with the large membrane-bound foci (Figure 4c, bottom).

3.5. RNA Synthesis by All Genera of Coronaviruses Takes Place in a Membrane-Bound Compartment

While the structure of ROs have been shown to be conserved across all genera of CoVs, some morphological differences between the viruses remain. Mainly, while convoluted membranes are found much more widely in alpha and beta CoV, they are found to a lesser extent in delta- and gamma-CoVs. In alpha- and beta-CoVs, the spherules were found associated with CM rather than zER and most spherules were in sealed compartments rather than remaining open to the cytosol, as is the case in most spherules in gamma-CoV infections [8]. Therefore, we sought to understand whether there might be any fundamental differences between the localization of sites of viral RNA synthesis in IBV compared with other CoV genera. Using one representative virus from each of the three other genera of CoVs (HCoV 229E (an alpha-CoV), SARS-CoV-2 (a beta-CoV), and PDCoV (a delta-CoV)), the location of nascent viral RNA labeled with BrU was assessed using TX100 and digitonin as before. Cells were labeled to detect BrU labeled nascent viral RNA or the viral nucleocapsid (N). While for each virus the N labeling (in red) was detected diffuse throughout the cytoplasm regardless of permeabilization method, BrU-labeled nascent viral RNA signal (in green) was contained within a membrane-bound compartment for HCoV 229E (Figure 5a), SARS-CoV-2 (Figure 5b), and PDCoV (Figure 5c). This is consistent with observations for IBV and demonstrates a conserved mechanism across the CoV family for viral RNA synthesis to be held within a membrane-bound compartment.

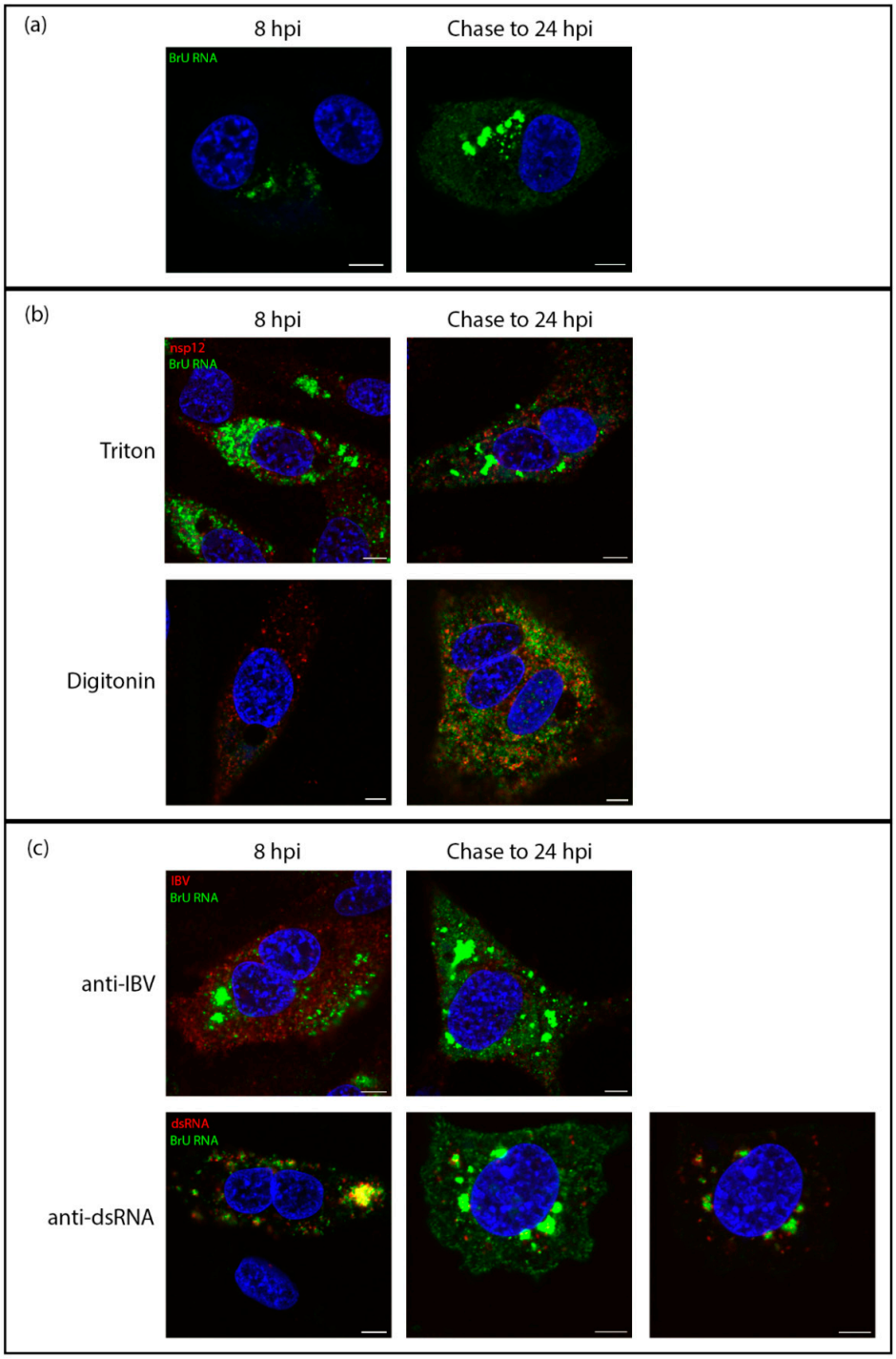

Figure 4. Viral RNA is transported to the cytoplasm later in infection. DF1 cells were infected with IBV. At 7 hpi cells were treated with BrU and ActD. At 8 hpi cells were either fixed (8 hpi) or chased with uridine until 24 hpi (chase to 24 hpi). (**a**) cells were then labeled for BrU (green), DAPI labeling the nuclei (blue). (**b**) DF1 cells infected with IBV were treated with BrU and ActD at 7 hpi then either fixed at 8 hpi or chased with uridine until 24hpi (chase to 24 hpi). Cells were permeabilized with Triton X-100 (top) or digitonin (bottom) then labelled for BrU (green) and nsp12 (red), DAPI labeling the nuclei (blue). (**c**) DF1 cells infected with IBV were treated with BrU and ActD at 7 hpi then either fixed at 8 hpi or chased with uridine until 24hpi (chase to 24 hpi). Cells were then labeled for BrU (green) and IBV (red; top) or dsRNA (red; bottom), DAPI labeling nuclei (blue). Scale bars represent 5 μm. Images are representative of three independent replicates.

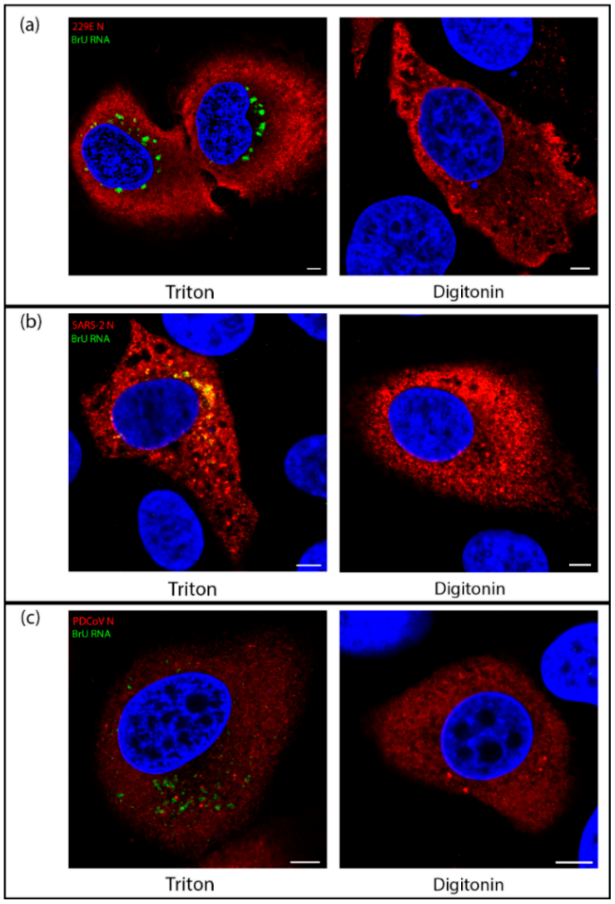

Figure 5. Viral RNA synthesis of diverse CoVs takes place within a membrane-bound compartment. (**a**) Huh7 cells were infected with HCoV 229E. At 7.5 hpi cells were treated with BrU and ActD for 30 min before fixation at 8 hpi. Cells were permeabilized with Triton X-100 (left) or digitonin (right) then labeled for BrU (green) and N (red), with DAPI labeling the nuclei (blue); (**b**) VeroE6 cells were infected with SARS-CoV-2. At 5.5 hpi, cells were treated with BrU and ActD for 30 min before fixation at 6 hpi. Cells were permeabilized with Triton X-100 (left) or digitonin (right) then labeled for BrU (green) and N (red), with DAPI labeling the nuclei (blue); (**c**) LLC-PK1 cells were infected with PDCoV. At 5.5 hpi, cells were treated with BrU and ActD for 30 min before fixation at 6 hpi. Cells were permeabilized with Triton X-100 (left) or digitonin (right) then labeled for BrU (green) and N (red), with DAPI labeling the nuclei (blue). Scale bars represent 5 µm. Images are representative of three independent replicates.

4. Discussion

The formation of ROs is conserved across all +RNA viruses, an essential step in their life cycle. These ROs have long been thought to provide a site for viral RNA synthesis and have been shown to do so for several viruses [8,30,31]. While these structures vary between the different virus families, there are many similarities, with the most basic of them being the energy required to rearrange cellular membranes to this extent. As obligate intracellular parasites, viruses are highly efficient and aim entirely to produce new generations of infectious particles as soon as possible. That these viruses induce these structures at all indicates that they are an important step in their life cycle [41,43]. The gammacoronavirus, IBV induces the formation of DMVs, zER and spherules which pinch out from, but remain tethered to the zER. While IBV DMVs were recently identified as a site for viral RNA synthesis, no role has yet been found for spherules [8].

Previous studies have shown for other +RNA viruses, such as SARS-CoV, FHV, and most recently in SARS-CoV-2, that dsRNA is found associated with DMVs [30,31,39,40]. In the current study we have shown using different permeabilization methods, that dsRNA is

found located within membrane-bound compartments. This is consistent with previous work [39] and suggests that dsRNA is also shielded within DMVs during IBV infection. Although a pore has recently been shown to be present in the DMV membrane [44], these are short lived/transient and have a diameter of 2–3 nm at their narrowest point, which would not be large enough to allow entry of an antibody complex of ~30 nm. It is worth noting however, that our data here cannot exclude the possibility of dsRNA association with spherules. The IBV spherule neck measured 4–5 nm [37], which would not be large enough to allow entry of an antibody complex. As dsRNA is a known target for intracellular pattern recognition receptors, it is likely that the virus aims to shield the dsRNA from detection within membrane-bound compartments such as DMVs. Indeed, activation of interferon (IFN) signaling is delayed following IBV infection and it was suggested that the IFN response seen later in IBV infection could be due to dsRNA "leaking" from DMVs [51]. However, this now does not seem to be the case, as data presented in the current work demonstrated that dsRNA was sealed within a membrane compartment at 24 hpi, a timepoint after which IFN signaling has been activated. Therefore, other mechanisms must exist to allow activation of IFN signaling later in IBV infection, and these remain to be elucidated.

Finding sites of coronavirus RNA synthesis has been a topic of much research in recent years. Using biochemical methods in vitro, it has been shown that SARS-CoV RNA synthesis takes place inside membrane-bound compartments [38]. More recently, it was shown that DMVs are the site of viral RNA synthesis during MERS-CoV and IBV replication [8]. However, the methods used in that study could not definitively show whether RNA synthesis takes place on the interior or cytoplasmic face of DMV membranes. A subsequent study showed that DMVs contain pores within the membrane connecting the interior of the vesicle with the cytoplasm [44], providing a route by which RNA synthesized inside DMVs could exit for translation or packaging. Despite this, the location of viral RNA synthesis either inside or on the outside of DMVs remained to be confirmed. Significantly, by employing both BrU labeling of nascent RNA and different permeabilization methods, we have shown that sites of coronavirus RNA synthesis are membrane protected. Therefore, we have demonstrated conclusively that viral RNA synthesis in fact takes place *within* a membrane-bound compartment. Moreover, we have confirmed that viral RNA synthesis by diverse CoVs from each of the four coronavirus genera, including recently identified SARS-CoV-2, takes place within a membrane-bound compartment. Although we cannot exclude that CoV RNA synthesis takes place when associated with spherules, as MERS-CoV and IBV RNA synthesis has been shown to be associated with DMVs [8], we can infer that RNA synthesis takes place *within* DMVs, and that this is conserved across the whole CoV family (Figure 6).

While it has previously been shown that newly synthesized IBV RNA location overlaps to some extent with the nsp14 [52], little else is known about the localization of viral proteins to sites of viral RNA synthesis. Several viral nsps are known to be involved in RO formation, including nsp3, nsp4, and nsp6 [39,41,43,53–55]; nsps are known to localize to DMVs and other RO membranes [34,39,56]. Here, we have shown that viral RNA is associated with dsRNA, but not with nsp12. While it was not surprising that as a replicative intermediate, dsRNA was found in close association with sites of viral RNA synthesis, the finding that nsp12 is not near these sites is somewhat surprising. However, this is likely to be since the antibody is unable to bind to nsp12 assembled within the replication/transcription complex (RTC) and actively involved in RNA synthesis. Nsp8 has been shown to interact with both the N- and C-terminal ends of nsp12 [57], which could very likely render the antigenic sites within nsp12 inaccessible to something as large as an antibody. Nsp12 further interacts directly with other viral proteins. MHV nsp12 interacts with nsp15 [58] and possibly with nsp5, nsp8, and nsp9 [59]. SARS-CoV nsp12 has been found in complex with nsp7, nsp8, and nsp14 [60]. Therefore, it is very likely that the nsp12 labeling detected here represents nsp12 that is not located within RTCs or is located within RTCs not actively involved in RNA synthesis. The amount of nsp12 signal detected that is presumably not

located within active RTCs is perhaps rather surprising. However, several nsps from other CoVs are known to localize to both DMVs and other RO membranes [34,39,56]. The role of non-RTC associated nsp12 during virus replication remains to be determined.

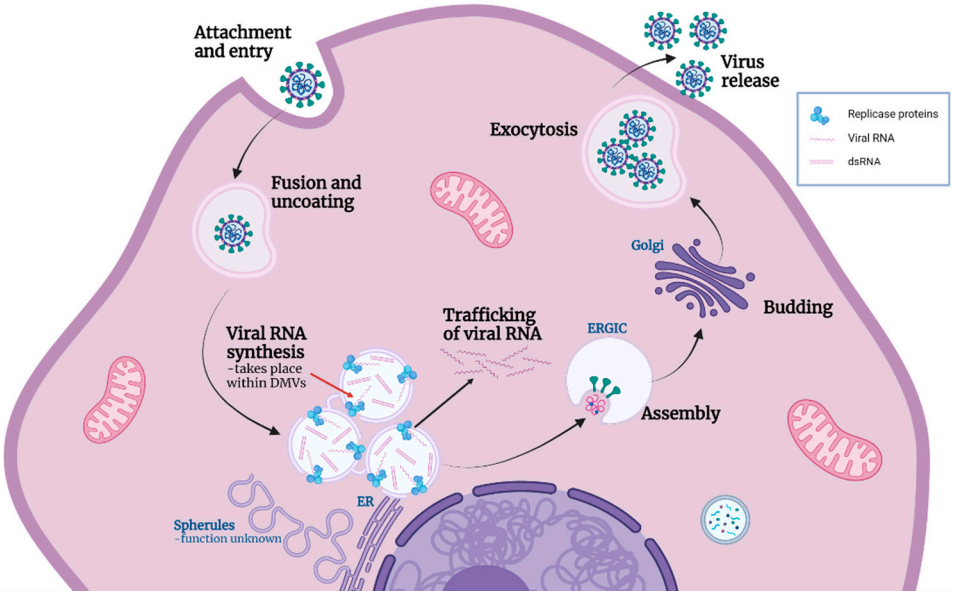

Figure 6. Model of coronavirus life cycle including functions of replication organelle. Coronaviruses (CoVs) attach to and enter cells where viral and cellular membranes fuse to uncoat the genomic RNA. CoV induces the formation of replication organelles (ROs): zippered ER and associated spherules, as well as convoluted membranes, which currently have an unknown function; and DMVs which are the site of viral RNA synthesis. Through the current work we can conclude that viral RNA synthesis occurs inside DMVs (red arrow). A proportion of the viral RNA is trafficked into the cytoplasm, while some remains within the DMVs along with dsRNA formed during replication. Recently identified pores provide the means for exit of viral RNA from DMVs. New virions assemble and bud into the ERGIC, followed by release from the cell by exocytosis. Figure created with Biorender.com.

Following characterization of the location of nascent RNA throughout infection, changes in the location of this RNA as infection progressed were studied. Using a pulse-chase approach, RNA synthesized between 7–8 hpi was visualized at 24 hpi. This demonstrated that by 24 hpi, viral RNA that was produced between 7–8 hpi showed two separate pools. The first remained in large, membrane-bound foci. These large accumulations of labeled viral RNA continued to associate with dsRNA within these compartments. The second pool of viral RNA produced between 7–8 hpi and tracked to 24 hpi had been exported into the cytoplasm. This pool of RNA was associated largely with structural proteins, presumably bound by N, or as it was being packaged into new virions and was consistent with the recently characterized pore in the DMV membrane [44]. These observations were consistent with a model whereby newly synthesized positive sense RNAs were exported out of the DMV to be translated or packaged, while positive and negative sense RNA templates remained within the DMVs for further rounds of RNA synthesis (Figure 6).

The CoV family contains many pathogens of animal and human interest. The RO of CoVs from all four genera have been confirmed previously to comprise DMVs and double membrane spherules. Here we investigated the site of viral RNA synthesis of one virus from each CoV genus. In all viruses we investigated (HCoV 229E, SARS-CoV-2, IBV, and PDCoV) the site of viral RNA synthesis was bound within a membrane, consistent with being located on the interior of DMVs [8,44]. Although experiments in the current work have been performed in continuous cell lines, considering that IBV ROs are conserved across a wide range of cell types, including ex vivo organ cultures [37,55,61], and that

observations here were conserved across the whole CoV family, it seems reasonable to hypothesize that sites of CoV RNA synthesis will be membrane protected in all cell types.

As summarized in Figure 6, the role of CoV induced convoluted membranes, zippered ER, and double membrane spherules remains elusive. However, knowing that all CoVs synthesize viral RNA within a membrane-bound compartment is a significant step in understanding the replication of this important virus family.

Supplementary Materials: The following are available online at https://www.mdpi.com/article/10.3390/v13122540/s1, Figure S1: Cellular transcription is inhibited with Actinomycin D treatment, Figure S2: Sites of viral RNA synthesis are associated with dsRNA but do not colocalize with nsp12., Video S1: Sites of viral RNA synthesis do not colocalize with nsp12; Video S2: Sites of viral RNA synthesis are associated with dsRNA.

Author Contributions: Conceptualization: H.J.M. and P.C.H; methodology: N.D., J.S., P.C.H. and H.J.M.; validation: N.D.; formal analysis: N.D.; investigation: N.D.; resources: N.D., P.C.H. and H.J.M.; data curation: N.D.; writing—original draft preparation: N.D. and H.J.M.; writing—review and editing: N.D., J.S., P.C.H. and H.J.M.; visualization: N.D.; supervision: H.J.M.; project administration: H.J.M.; funding acquisition: H.J.M. All authors have read and agreed to the published version of the manuscript.

Funding: This research was funded by Biotechnology and Biological Sciences Research Council, grant numbers BB/N002350/1, BBS/E/I/00002535, BBS/E/I/00007034, BBS/E/I/00007038, and BBS/E/I/00007039.

Acknowledgments: The authors would like to thank Linda Saif, Ohio State University, for kindly providing porcine deltacoronavirus for use in this work. We would also like to thank Miles Carroll, UK Health Security Agency, for kindly sharing SARS-CoV-2, hCov-19/England/02/2020.

Conflicts of Interest: The authors declare no conflict of interest. The funders had no role in the design of the study; in the collection, analyses, or interpretation of data; in the writing of the manuscript, or in the decision to publish the results.

References

1. Ksiazek, T.G.; Erdman, D.; Goldsmith, C.S.; Zaki, S.R.; Peret, T.; Emery, S.; Tong, S.; Urbani, C.; Comer, J.A.; Lim, W.; et al. A Novel Coronavirus Associated with Severe Acute Respiratory Syndrome. *N. Engl. J. Med.* **2003**, *348*, 1953–1966. [CrossRef] [PubMed]
2. Zaki, A.M.; Van Boheemen, S.; Bestebroer, T.M.; Osterhaus, A.D.M.E.; Fouchier, R.A.M. Isolation of a Novel Coronavirus from a Man with Pneumonia in Saudi Arabia. *N. Engl. J. Med.* **2012**, *367*, 1814–1820. [CrossRef]
3. W.H.O. World Health Oganisation (WHO) Coronavirus (COVID-19) Dashboard With Vaccination Data. August 2021. Available online: https://covid19.who.int (accessed on 17 December 2021).
4. Zhou, P.; Yang, X.-L.; Wang, X.-G.; Hu, B.; Zhang, L.; Zhang, W.; Si, H.-R.; Zhu, Y.; Li, B.; Huang, C.-L.; et al. A pneumonia outbreak associated with a new coronavirus of probable bat origin. *Nature* **2020**, *579*, 270–273. [CrossRef]
5. Miller, S.; Krijnse-Locker, J. Modification of intracellular membrane structures for virus replication. *Nat. Rev. Microbiol.* **2008**, *6*, 363–374. [CrossRef]
6. Nagy, P.D.; Strating, J.R.P.M.; Van Kuppeveld, F.J.M. Building Viral Replication Organelles: Close Encounters of the Membrane Types. *PLOS Pathog.* **2016**, *12*, e1005912. [CrossRef] [PubMed]
7. Netherton, C.L.; Wileman, T. Virus factories, double membrane vesicles and viroplasm generated in animal cells. *Curr. Opin. Virol.* **2011**, *1*, 381–387. [CrossRef]
8. Snijder, E.J.; Limpens, R.W.A.L.; de Wilde, A.H.; de Jong, A.W.M.; Zevenhoven-Dobbe, J.C.; Maier, H.J.; Faas, F.F.G.A.; Koster, A.J.; Bárcena, M. A unifying structural and functional model of the coronavirus replication organelle: Tracking down RNA synthesis. *PLoS Biol.* **2020**, *18*, e3000715. [CrossRef]
9. Gosert, R.; Kanjanahaluethai, A.; Egger, D.; Bienz, K.; Baker, S.C. RNA Replication of Mouse Hepatitis Virus Takes Place at Double-Membrane Vesicles. *J. Virol.* **2002**, *76*, 3697–3708. [CrossRef]
10. Den Boon, J.A.; Ahlquist, P. Organelle-Like Membrane Compartmentalization of Positive-Strand RNA Virus Replication Factories. *Annu. Rev. Microbiol.* **2010**, *64*, 241–256. [CrossRef]
11. Neufeldt, C.; Joyce, M.A.; Van Buuren, N.; Levin, A.; Kirkegaard, K.; Gale, M., Jr.; Tyrrell, D.L.J.; Wozniak, R.W. The Hepatitis C Virus-Induced Membranous Web and Associated Nuclear Transport Machinery Limit Access of Pattern Recognition Receptors to Viral Replication Sites. *PLOS Pathog.* **2016**, *12*, e1005428. [CrossRef] [PubMed]
12. Nagy, P.D.; Lin, W. Taking over Cellular Energy-Metabolism for TBSV Replication: The High ATP Requirement of an RNA Virus within the Viral Replication Organelle. *Viruses* **2020**, *12*, 56. [CrossRef]

13. Harak, C.; Lohmann, V. Ultrastructure of the replication sites of positive-strand RNA viruses. *Virology* **2015**, *479-480*, 418–433. [CrossRef] [PubMed]
14. Paul, D.; Bartenschlager, R. Architecture and biogenesis of plus-strand RNA virus replication factories. *World J. Virol.* **2013**, *2*, 32–48. [CrossRef]
15. Vila-Pérez, G.; Rejas, M.T.; Rodríguez, D. Ultrastructural characterization of membranous torovirus replication factories. *Cell. Microbiol.* **2016**, *18*, 1691–1708. [CrossRef] [PubMed]
16. Gosert, R.; Egger, D.; Lohmann, V.; Bartenschlager, R.; Blum, H.E.; Bienz, K.; Moradpour, D. Identification of the Hepatitis C Virus RNA Replication Complex in Huh-7 Cells Harboring Subgenomic Replicons. *J. Virol.* **2003**, *77*, 5487–5492. [CrossRef]
17. Monaghan, P.; Cook, H.; Jackson, T.; Ryan, M.D.; Wileman, T. The ultrastructure of the developing replication site in foot-and-mouth disease virus-infected BHK-38 cells. *J. Gen. Virol.* **2004**, *85*, 933–946. [CrossRef]
18. Belov, G.A.; Nair, V.; Hansen, B.T.; Hoyt, F.H.; Fischer, E.R.; Ehrenfeld, E. Complex Dynamic Development of Poliovirus Membranous Replication Complexes. *J. Virol.* **2011**, *86*, 302–312. [CrossRef]
19. Limpens, R.W.A.L.; van der Schaar, H.M.; Kumar, D.; Koster, A.J.; Snijder, E.J.; van Kuppeveld, F.J.; Bárcena, M. The Transformation of Enterovirus Replication Structures: A Three-Dimensional Study of Single- and Double-Membrane Compartments. *mBio* **2011**, *2*, e00166-11. [CrossRef]
20. Melia, C.E.; Peddie, C.J.; de Jong, A.; Snijder, E.J.; Collinson, L.M.; Koster, A.J.; van der Schaar, H.M.; van Kuppeveld, F.J.M.; Bárcena, M. Origins of Enterovirus Replication Organelles Established by Whole-Cell Electron Microscopy. *mBio* **2019**, *10*, e00951-19. [CrossRef]
21. Cortese, M.; Goellner, S.; Acosta, E.G.; Neufeldt, C.; Oleksiuk, O.; Lampe, M.; Haselmann, U.; Funaya, C.; Schieber, N.; Ronchi, P.; et al. Ultrastructural Characterization of Zika Virus Replication Factories. *Cell Rep.* **2017**, *18*, 2113–2123. [CrossRef] [PubMed]
22. Gillespie, L.K.; Hoenen, A.; Morgan, G.; Mackenzie, J.M. The Endoplasmic Reticulum Provides the Membrane Platform for Biogenesis of the Flavivirus Replication Complex. *J. Virol.* **2010**, *84*, 10438–10447. [CrossRef] [PubMed]
23. Offerdahl, D.K.; Dorward, D.W.; Hansen, B.T.; Bloom, M.E. A Three-Dimensional Comparison of Tick-Borne Flavivirus Infection in Mammalian and Tick Cell Lines. *PLoS ONE* **2012**, *7*, e47912. [CrossRef]
24. Welsch, S.; Miller, S.; Romero-Brey, I.; Merz, A.; Bleck, C.K.E.; Walther, P.; Fuller, S.D.; Antony, C.; Krijnse-Locker, J.; Bartenschlager, R. Composition and Three-Dimensional Architecture of the Dengue Virus Replication and Assembly Sites. *Cell Host Microbe* **2009**, *5*, 365–375. [CrossRef] [PubMed]
25. Schwartz, M.; Chen, J.; Lee, W.-M.; Janda, M.; Ahlquist, P. Alternate, virus-induced membrane rearrangements support positive-strand RNA virus genome replication. *Proc. Natl. Acad. Sci. USA* **2004**, *101*, 11263–11268. [CrossRef] [PubMed]
26. Grimley, P.M.; Berezesky, I.K.; Friedman, R.M. Cytoplasmic Structures Associated with an Arbovirus Infection: Loci of Viral Ribonucleic Acid Synthesis. *J. Virol.* **1968**, *2*, 1326–1338. [CrossRef]
27. Grimley, P.M.; Levin, J.G.; Berezesky, I.K.; Friedman, R.M. Specific Membranous Structures Associated with the Replication of Group A Arboviruses. *J. Virol.* **1972**, *10*, 492–503. [CrossRef]
28. Kujala, P.; Ikäheimonen, A.; Ehsani, N.; Vihinen, H.; Auvinen, P.; Kaääriàinen, L. Biogenesis of the Semliki Forest Virus RNA Replication Complex. *J. Virol.* **2001**, *75*, 3873–3884. [CrossRef]
29. Miller, D.J.; Schwartz, M.D.; Ahlquist, P. Flock House Virus RNA Replicates on Outer Mitochondrial Membranes in Drosophila Cells. *J. Virol.* **2001**, *75*, 11664–11676. [CrossRef]
30. Ertel, K.J.; Benefield, D.; Castaño-Diez, D.; Pennington, J.G.; Horswill, M.; den Boon, J.A.; Otegui, M.S.; Ahlquist, P. Cryo-electron tomography reveals novel features of a viral RNA replication compartment. *eLife* **2017**, *6*, e25940. [CrossRef]
31. Kopek, B.; Perkins, G.; Miller, D.J.; Ellisman, M.H.; Ahlquist, P. Three-Dimensional Analysis of a Viral RNA Replication Complex Reveals a Virus-Induced Mini-Organelle. *PLoS Biol.* **2007**, *5*, e220. [CrossRef]
32. De Wilde, A.H.; Raj, V.S.; Oudshoorn, D.; Bestebroer, T.M.; van Nieuwkoop, S.; Limpens, R.W.; Posthuma, C.C.; van der Meer, Y.; Bárcena, M.; Haagmans, B.L.; et al. MERS-coronavirus replication induces severe in vitro cytopathology and is strongly inhibited by cyclosporin A or interferon-α treatment. *J. Gen. Virol.* **2013**, *94 Pt 8*, 1749–1760. [CrossRef]
33. Goldsmith, C.S.; Tatti, K.M.; Ksiazek, T.G.; Rollin, P.; Comer, J.A.; Lee, W.W.; Rota, P.A.; Bankamp, B.; Bellini, W.J.; Zaki, S.R. Ultrastructural Characterization of SARS Coronavirus. *Emerg. Infect. Dis.* **2004**, *10*, 320–326. [CrossRef]
34. Snijder, E.J.; van der Meer, Y.; Zevenhoven-Dobbe, J.; Onderwater, J.J.; Van Der Meulen, J.; Koerten, H.K.; Mommaas, A.M. Ultrastructure and Origin of Membrane Vesicles Associated with the Severe Acute Respiratory Syndrome Coronavirus Replication Complex. *J. Virol.* **2006**, *80*, 5927–5940. [CrossRef] [PubMed]
35. Zhou, X.; Cong, Y.; Veenendaal, T.; Klumperman, J.; Shi, D.; Mari, M.; Reggiori, F. Ultrastructural Characterization of Membrane Rearrangements Induced by Porcine Epidemic Diarrhea Virus Infection. *Viruses* **2017**, *9*, 251. [CrossRef] [PubMed]
36. Doyle, N.; Hawes, P.C.; Simpson, J.; Adams, L.H.; Maier, H.J. The Porcine Deltacoronavirus Replication Organelle Comprises Double-Membrane Vesicles and Zippered Endoplasmic Reticulum with Double-Membrane Spherules. *Viruses* **2019**, *11*, 1030. [CrossRef] [PubMed]
37. Maier, H.; Hawes, P.C.; Cottam, E.M.; Mantell, J.; Verkade, P.; Monaghan, P.; Wileman, T.; Britton, P. Infectious Bronchitis Virus Generates Spherules from Zippered Endoplasmic Reticulum Membranes. *mBio* **2013**, *4*, e00801-13. [CrossRef] [PubMed]

38. Van Hemert, M.J.; van den Worm, S.H.E.; Knoops, K.; Mommaas, A.M.; Gorbalenya, A.E.; Snijder, E.J. SARS-Coronavirus Replication/Transcription Complexes Are Membrane-Protected and Need a Host Factor for Activity In Vitro. *PLOS Pathogens* **2008**, *4*, e1000054. [CrossRef] [PubMed]
39. Knoops, K.; Kikkert, M.; Worm, S.H.E.V.D.; Zevenhoven-Dobbe, J.C.; Van Der Meer, Y.; Koster, A.J.; Mommaas, A.M.; Snijder, E.J. SARS-Coronavirus Replication Is Supported by a Reticulovesicular Network of Modified Endoplasmic Reticulum. *PLoS Biol.* **2008**, *6*, e226. [CrossRef] [PubMed]
40. Klein, S.; Cortese, M.; Winter, S.L.; Wachsmuth-Melm, M.; Neufeldt, C.J.; Cerikan, B.; Stanifer, M.L.; Boulant, S.; Bartenschlager, R.; Chlanda, P. SARS-CoV-2 structure and replication characterized by in situ cryo-electron tomography. *Nat. Commun.* **2020**, *11*, 5885. [CrossRef]
41. Gadlage, M.J.; Sparks, J.S.; Beachboard, D.C.; Cox, R.G.; Doyle, J.D.; Stobart, C.; Denison, M.R. Murine Hepatitis Virus Nonstructural Protein 4 Regulates Virus-Induced Membrane Modifications and Replication Complex Function. *J. Virol.* **2010**, *84*, 280–290. [CrossRef]
42. Van der Meer, Y.; Snijder, E.J.; Dobbe, C.J.; Schleich, S.; Denison, R.M.; Spaan, J.W.; Locker, K.J. Localization of Mouse Hepatitis Virus Nonstructural Proteins and RNA Synthesis Indicates a Role for Late Endosomes in Viral Replication. *J. Virol.* **1999**, *73*, 7641–7657. [CrossRef]
43. Lundin, A.; Dijkman, R.; Bergström, T.; Kann, N.; Adamiak, B.; Hannoun, C.; Kindler, E.; Jonsdottir, H.R.; Muth, D.; Kint, J.; et al. Targeting Membrane-Bound Viral RNA Synthesis Reveals Potent Inhibition of Diverse Coronaviruses Including the Middle East Respiratory Syndrome Virus. *PLOS Pathog.* **2014**, *10*, e1004166. [CrossRef]
44. Wolff, G.; Limpens, R.W.A.L.; Zevenhoven-Dobbe, J.C.; Laugks, U.; Zheng, S.; De Jong, A.W.M.; Koning, R.I.; Agard, D.A.; Grünewald, K.; Koster, A.J.; et al. A molecular pore spans the double membrane of the coronavirus replication organelle. *Science* **2020**, *369*, 1395–1398. [CrossRef]
45. Casais, R.; Thiel, V.; Siddell, S.G.; Cavanagh, D.; Britton, P. Reverse Genetics System for the Avian Coronavirus Infectious Bronchitis Virus. *J. Virol.* **2001**, *75*, 12359–12369. [CrossRef]
46. Hull, R.N.; Cherry, W.R.; Weaver, G.W. The origin and characteristics of a pig kidney cell strain, LLC-PK1. *Vitr. Cell. Dev. Biol. Anim.* **1976**, *12*, 670–677. [CrossRef] [PubMed]
47. Hu, H.; Jung, K.; Vlasova, A.N.; Chepngeno, J.; Lu, Z.; Wang, Q.; Saif, L.J. Isolation and Characterization of Porcine Deltacoronavirus from Pigs with Diarrhea in the United States. *J. Clin. Microbiol.* **2015**, *53*, 1537–1548. [CrossRef]
48. Jung, K.; Hu, H.; Eyerly, B.; Lu, Z.; Chepngeno, J.; Saif, L.J. Pathogenicity of 2 Porcine Deltacoronavirus Strains in Gnotobiotic Pigs. *Emerg. Infect. Dis.* **2015**, *21*, 650–654. [CrossRef]
49. Hagemeijer, M.C.; Vonk, A.M.; Monastyrska, I.; Rottier, P.J.M.; de Haan, C. Visualizing Coronavirus RNA Synthesis in Time by Using Click Chemistry. *J. Virol.* **2012**, *86*, 5808–5816. [CrossRef] [PubMed]
50. Hackbart, M.; Deng, X.; Baker, S.C. Coronavirus endoribonuclease targets viral polyuridine sequences to evade activating host sensors. *Proc. Natl. Acad. Sci. USA* **2020**, *117*, 8094–8103. [CrossRef] [PubMed]
51. Kint, J.; Fernandez-Gutierrez, M.M.; Maier, H.; Britton, P.; Langereis, M.A.; Koumans, J.; Wiegertjes, G.F.; Forlenza, M. Activation of the Chicken Type I Interferon Response by Infectious Bronchitis Coronavirus. *J. Virol.* **2015**, *89*, 1156–1167. [CrossRef]
52. Xu, L.; Khadijah, S.; Fang, S.; Wang, L.; Tay, F.P.L.; Liu, D.X. The Cellular RNA Helicase DDX1 Interacts with Coronavirus Nonstructural Protein 14 and Enhances Viral Replication. *J. Virol.* **2010**, *84*, 8571–8583. [CrossRef]
53. Beachboard, D.C.; Anderson-Daniels, J.M.; Denison, M.R. Mutations across Murine Hepatitis Virus nsp4 Alter Virus Fitness and Membrane Modifications. *J. Virol.* **2014**, *89*, 2080–2089. [CrossRef] [PubMed]
54. Clementz, M.A.; Kanjanahaluethai, A.; O'Brien, T.E.; Baker, S.C. Mutation in murine coronavirus replication protein nsp4 alters assembly of double membrane vesicles. *Virology* **2008**, *375*, 118–129. [CrossRef]
55. Doyle, N.; Neuman, B.W.; Simpson, J.; Hawes, P.C.; Mantell, J.; Verkade, P.; Alrashedi, H.; Maier, H.J. Infectious Bronchitis Virus Nonstructural Protein 4 Alone Induces Membrane Pairing. *Viruses* **2018**, *10*, 477. [CrossRef] [PubMed]
56. Hagemeijer, M.C.; Monastyrska, I.; Griffith, J.; van der Sluijs, P.; Voortman, J.; van Bergen en Henegouwen, P.M.; Vonk, A.M.; Rottier, P.J.; Reggiori, F.; de Haan, C.A. Membrane rearrangements mediated by coronavirus nonstructural proteins 3 and 4. *Virology* **2014**, *458–459*, 125–135. [CrossRef]
57. Tan, Y.W.; Fung, T.S.; Shen, H.; Huang, M.; Liu, D.X. Coronavirus infectious bronchitis virus non-structural proteins 8 and 12 form stable complex independent of the non-translated regions of viral RNA and other viral proteins. *Virology* **2017**, *513*, 75–84. [CrossRef]
58. Athmer, J.; Fehr, A.; Grunewald, M.; Smith, E.C.; Denison, M.; Perlman, S. In Situ Tagged nsp15 Reveals Interactions with Coronavirus Replication/Transcription Complex-Associated Proteins. *mBio* **2017**, *8*, e02320-16. [CrossRef]
59. Brockway, S.M.; Lu, X.T.; Peters, T.R.; Dermody, T.S.; Denison, M.R. Intracellular Localization and Protein Interactions of the Gene 1 Protein p28 during Mouse Hepatitis Virus Replication. *J. Virol.* **2004**, *78*, 11551–11562. [CrossRef] [PubMed]
60. Subissi, L.; Posthuma, C.C.; Collet, A.; Zevenhoven-Dobbe, J.C.; Gorbalenya, A.; Decroly, E.; Snijder, E.; Canard, B.; Imbert, I. One severe acute respiratory syndrome coronavirus protein complex integrates processive RNA polymerase and exonuclease activities. *Proc. Natl. Acad. Sci. USA* **2014**, *111*, E3900–E3909. [CrossRef]
61. Maier, H.J.; Neuman, B.; Bickerton, E.; Keep, S.M.; Alrashedi, H.; Hall, R.; Britton, P. Extensive coronavirus-induced membrane rearrangements are not a determinant of pathogenicity. *Sci. Rep.* **2016**, *6*, 27126. [CrossRef]